An in-cell approach to evaluate E3 ligases for use in targeted protein degradation

Yunan Zheng[1,$], Anamika Singh[2,$], Zeqi Niu[1], Violeta Marin[1], Jonathon Young[1], Paul Richardson[1], Marcus L. Hemshorn[2], Richard B. Cooley[2], P. Andrew Karplus[2], Kedar Puvar[1], Scott E. Warder[1], Anil Vasudevan[1], Justin M. Reitsma[1*], Ryan A. Mehl[2*]

[1] Technology & Therapeutic Platforms, AbbVie Inc., North Chicago, Illinois 60064, USA
[2] Department of Biochemistry and Biophysics and GCE4All Research Center, Oregon State University, Corvallis, OR 97331, USA.
[$] Y.Z. and A.S. contributed equally to this work

*email: yunan.zheng@abbvie.com; justin.m.reitsma@abbvie.com; ryan.mehl@oregonstate.edu,

Abstract

A major challenge in evaluating the suitability of the ~700 known and putative E3 ligases for target protein degradation (TPD) is the lack of ligase-specific binders. Here, we use genetic code expansion (GCE) to express in living cells an E3 ligase with a site-specifically encoded, tetrazine-containing non-canonical amino acid (Tet-ncAA). Then, using click chemistry, we conjugate the incorporated Tet with a strained trans-cyclooctene (sTCO) tethered to a neo-substrate protein binder. The resulting covalent E3 ligase–binder construct can then be evaluated for TPD of the neo-substrate. We first demonstrate that cereblon (CRBN) has a rather high plasticity for TPD by studying CRBN containing a Tet-ncAA at a variety of surface positions. When these CRBN forms are covalently tethered to an sTCO-linker-JQ1 reagent, they all successfully recruit BRD2/4 for degradation, with the efficiency depending on the placement of the Tet-ncAA and the linker length. The results highlight the ability of this approach to map E3 surfaces and identify optimal TPD interfaces and pockets. Applying this strategy to SPOP, an E3 ligase with no known specific ligand, we demonstrate that multiple sites on its surface can support TPD, revealing potential for PROTAC-type development. This E3-ligand-free degrader (ELF-degrader) platform preserves the native state of E3 ligases, enables the interrogation of any E3 surface region in live cells, and is applicable to a broad range of E3 ligases. ELF-degraders represent a versatile approach to define functional degron sites, guide degrader design, and unlock new E3 ligases – those without known ligands – for therapeutic applications.

Keywords: ubiquitin-proteasome system, targeted protein degradation, E3 ligases, cereblon, SPOP, genetic code expansion, tetrazine click chemistry

Introduction

A healthy cell maintains an exquisite balance of the synthesis and degradation rates of its various proteins via a set of complex processes that together are known as proteostasis (i.e. protein homeostasis). This governing of the integrity of the cellular proteome involves controlling multiple interconnected pathways responsible for protein synthesis, folding, transport, and disposal[1-3]. And many diseases, including cancer, neurological conditions, metabolic diseases, and age-related pathologies have been linked to dysregulated proteostasis [4-6].

In eukaryotes, one key process of proteostasis is the ubiquitin-proteasome system (UPS), in which added ubiquitin tags targets specific damaged, misfolded, or no longer needed proteins for proteasomal degradation [7]. The discovery of the UPS was recognized by the 2004 Nobel prize in chemistry [8], and numerous studies have highlighted its importance for cellular health [9-11], and [12]). The UPS-mediated protein degradation pathway requires the coordination of ubiquitin-activating enzymes (E1), ubiquitin-conjugating enzymes (E2), and ubiquitin-protein ligases (E3). E3 ligases recognize targets through degrons and facilitate the transfer of ubiquitin. Based on their mechanisms of ubiquitin transfer and domain architecture, E3 ligases can be classified into three main families [13]: the RING (really interesting new gene) finger family, the HECT (homologous to E6AP C-terminus) family, and the "RING-between-RING" (RBR) family. The RING finger subfamily called Cullin-RING ligases (CRLs) makes up over 40% of all E3 ligases. CRLs are modular enzymes that consist of four components: a scaffold cullin protein, a RING finger protein for engaging an E2 enzyme, a substrate receptor for target recognition, and adaptor proteins linking the receptor to cullin[14-16]. The most widely recognized CRL is cereblon (CRBN), which functions as the substrate receptor for the CRL4 complex (Fig. 1a).

Over the past two decades, effective therapeutics have been developed that coopt the UPS to degrade specific disease-causing proteins [17-18], and these powerful targeted protein degradation (TPD) strategies often target otherwise "undruggable" proteins [19-21]. One approach involves small molecule "molecular glue" compounds [22-24] which bind tightly to an E3 ligase, changing its surface in ways that create a binding site for another protein which when bound gets ubiquitinated and targeted for degradation (Fig. 1b). Classic examples are immunomodulatory drugs (IMiDs) like thalidomide that "glue" the E3 ligase CRBN to certain transcription factors [25-27] and cause their proteasome-dependent degradation [19, 26, 28-29]. A more versatile TPD approach using proteolysis-targeting chimeras (PROTACs) was developed by Sakamoto *et al.* [30]. PROTAC molecules consist of a linker connecting a ligand for a specific E3 ligase with a ligand for a target protein of choice, which brings the target proteins close to the E3 ligase (Fig. 1b) and leads to the ubiquitination of the target protein [31-32].

Thus far TPD applications have been limited to using just a dozen of the ~700 human E3 ligases [33-35], because there are only a few for which specific ligand binding sites and high-affinity ligands have been identified [36-37]. The main "workhorses" are CRBN and the von Hippel-Lindau (VHL) E3 ligases; these are both well characterized, have known tight-binding ligands, and have been successfully redirected to degrade hundreds of proteins [20, 38]. Despite these therapeutic advances, we still know very little about the structural constraints required for E3-guided protein degradation including which potential surface locations on E3 ligases are amenable for developing molecular glue type therapies.

The current state-of-the-art to validate E3 ligases for TPD relies on either 1) engineering the ligase with protein tags to allow tag-induced proximity that brings E3 ligase and target protein in proximity upon strong interaction of the protein tags (e.g., HaloTag/FKBP12, dTAG, aTAG or GFP nanobody) [39-41] or 2) producing a recombinant E3 ligase and covalently functionalizing it *in vitro* with a neo-substrate protein binder based on cysteine-maleimide *co*valent modification *f*ollowed by *E*3 *e*lectroporation (COFFEE) back into cells [36, 42]. The limitations of protein tag-induced proximity are that site-specificity cannot be controlled and the bulky 15~30 kDa protein tags that are restricted to N- or C-termini attachment. While COFFEE involves a less-perturbing modification of E3 ligases, only those that can be purified, labeled efficiently on a single cysteine and returned into functional cellular UPS complexes can be explored. Due to these limitations, neither approach can shed light on the structural plasticity and potential ligand binding sites of the untapped E3 ligases.

Since genetic code expansion (GCE) [43-46] using non-canonical amino acids (ncAAs) can preserve intracellular ligase function and allow for residue-specific introduction of click-chemistry ligation sites, GCE presents an avenue to overcome the above limitations. Indeed, by exploiting the tetrazine (Tet) – transcyclooctene (TCO) click-chemistry reaction which gives rapid, quantitative ligation within live eukaryotic cells [47], it should be possible to position a Tet ncAA anywhere on the surface of an E3 protein, allowing one to survey the surface and map areas that are optimal for generating protein complexes that lead to degradation. If proven correct, this approach could be applied universally to all E3 ligases for exploring not only their potential for neo-substrate TPD, but also their "hot pockets" to gain confidence for chemistry campaign to generate a specific binder. In this approach, the live cells containing E3-Tet proteins would initiate target protein degradation when exposed to a strained TCO (sTCO) reagent attached to a variable linker and a ligand specific for a target protein (Fig. 1c). We call this an E3-ligand free-Degrader or ELF-Degrader approach.

Here, we test this ELF-Degrader approach in a human cell line by evaluating the TPD efficiencies of multiple Tet surface positions of the E3-ligase CRBN reacted with an sTCO-fused JQ1, a ligand used in the successful PROTAC work targeting the neo-substrates BRD2 and BRD4 [46, 48]. We discover a remarkably high level of plasticity with regard to the surfaces of CRBN that can direct efficient protein degradation using ELF-Degraders, with longer linkers (within the range tested) generally performing better. We then applied this ELF-Degrader approach to Speckle-type POZ protein (SPOP), a tumor suppressor and well-studied member of the MATHBTB E3 ligase family[49-50] which has not been used for TPD due to a lack of known tight-binding ligands. The results reveal multiple SPOP surface sites that can promote TPD, and thus demonstrate the utility of the ELF-degrader approach to identify E3 ligase surfaces that hold promise for developing TPD-promoting ligands.

RESULTS

Strategy for development of a GCE-based E3-ligand free TPD

As a model system for developing the ELF-Degrader approach to TPD (Fig. 1c), we sought to recapitulate the efficient CRBN-mediated ubiquitination and proteasomal degradation of the bromodomains BRD2 and BRD4 (BRD2/4) that is induced by the dBET6 PROTAC molecule – a chimera with the BRD2/4 ligand JQ1 conjugated to the CRBN binder pomalidomide [51]. For the E3 anchor chemistry, we chose the 2-amino-3-(3-(6-butyl-1,2,4,5-tetrazin-3-yl)phenyl) propanoic acid non-canonical amino acid (Tet3Bu; Fig. 2a) since it incorporates well in HEK293T cells, undergoes rapid in-cell click reactions with cell permeable sTCO reagents [47],

and its on-protein reactivity can be readily assessed by the fraction of protein undergoing a gel mobility shift after an *in vitro* reaction with an sTCO-PEG$_{5K}$ polymer [52-53]

The GCE system for efficiently expressing Tet3Bu-containing proteins in HEK293T cells [47] includes two plasmids, one expressing the Tet3Bu-specific aaRS, the other expressing the target protein for Tet3Bu incorporation, and both expressing the amber stop codon (TAG) suppressing cognate tRNA for the aaRS (Fig. 2b). Target proteins for Tet3Bu incorporation were either a sfGFP-N150TAG (sfGFP^{150}) test protein, or a CRBN$^{\#}$ protein, with the superscripts denoting the residue for Tet3Bu incorporation. C- or N-terminal FLAG tags were added to enable identification in western blots, and for testing expression and reaction conditions. For use as a control, an additional version of the second plasmid encodes wild type CRBN (CRBN^{WT}).

For the click-chemistry ELF-degrader ligation reagents, we designed six chimeric "sTCO-JQ1 degraders" (Fig. 2c) linking a reactive sTCO group with the JQ1 BRD2/4 ligand [46, 48]. Linkers ranged from a 2-carbon chain (C2) up to 5 ethylene glycol groups (PEG5) to provide flexibility for how the neo-substrate BRD2/4 was presented to CRBN. In describing these reagents, we use "JQ1" to refer to the bioactive (+)JQ1 stereochemistry and "(-)JQ1" to refer to the inactive enantiomer.

ELF degrader recruitment of BRD2/4 as a CRBN neosubstrate

In generating CRBN^{Tet} mutants to test for promoting TPD through reaction with sTCO-JQ1 degraders, we first picked five sites around the known IMiD-binding pocket of CRBN (residues 353, 355, 376, 377, 388) thinking that they would best mimic the TPD function of the dBET6 PROTAC molecule, along with one contrasting site (residue 70) that is far both from the IMiD-binding pocket and predicted protein interactions (Fig. 2d).

Expression and high-yield in-cell reactivity of containing CRBN^{Tet} forms
To test the ability of this GCE system to make Tet-containing proteins in the HEK293T cells, we co-transfected cells with the Tet3Bu-RS plasmid along with a plasmid encoding either sfGFP^{150}, a CRBN^{Tet} form or CRBN^{WT} (Fig. 2b). To confirm the expression and reactivity of the Tet-containing proteins, we cultured the cells in the presence and absence of Tet3Bu, lysed the cells and reacted some lysate with sTCO-PEG$_{5K}$ (Fig. 3a,b). These results demonstrated the robustness of the expression system, with full-length expression of the sfGFP control and the CRBN^{Tet} forms dependent on the presence of Tet3Bu, and all CRBN^{Tet} forms expressed at levels similar to that of CRBN^{WT}. Also, for the Tet-containing proteins, full reactivity was evident, as >95% of each protein was shifted to a higher molecular weight, whereas the control CRBN^{WT} control remained unshifted (Fig. 3b). Based on that success, we carried out the same tests in HEK293T CRBN knockout (K/O) cells. Again, all proteins expressed well with Tet3Bu incorporated, although with a somewhat greater variation in amounts, and they reacted quantitatively *in vitro* with sTCO-PEG$_{5K}$ (Fig. S1). We conclude that in both cell lines this GCE system gives full incorporation of a reactive Tet ncAA into each CRBN mutant.

Next, before assessing reactions inside mammalian cells, we reacted the sTCO-C2-JQ1 degrader *in vitro* with purified Tet-containing sfGFP^{150} to test the ability of the degraders to ligate Tet-containing proteins. Importantly, since reaction with a sTCO-JQ1 degrader will block a later reaction with sTCO-PEG$_{5K}$, a simple assay we use throughout this study for the completeness of reaction with a degrader is the lack of a mobility shift upon subsequent reaction with sTCO-PEG$_{5K}$. This mobility shift assay showed that a 15-minute reaction using

3-equivalents of the sTCO-C2-JQ1 degrader led to complete labeling (Fig. S2a), and the integrity of the product was confirmed by mass spectrometry (Fig. S2b).

To achieve quantitative in-cell labeling of Tet-proteins using the sTCO-JQ1 degraders, we used $CRBN^{355}$ as the test protein, and sought conditions which fully blocked the subsequent reaction – after cell lysis – with sTCO-PEG_{5K} (Fig. 3c,d). Trying degrader concentrations of 0.01, 0.1 and 1 μM and incubation times of 1 h and 6 h, we found that only a 6 h incubation at 1 μM of sTCO-JQ1 degrader gave complete labeling of $CRBN^{355}$, and that these conditions worked across all linker lengths (Fig. 3d). At 0.01 and 0.1 μM degrader concentrations, the fraction of $CRBN^{Tet}$ labeled appeared to be roughly 10% and 50%, respectively (Fig. S3).

ELF degraders applied to multiple $CRBN^{Tet}$ forms direct the degradation of BRD2/4

Since $CRBN^{Tet}$ expression requires the simultaneous transient transfection of two plasmids, a subset of cells will not express any $CRBN^{Tet}$ protein, and thus will not exhibit any ELF degrader-dependent TPD. To avoid considering these cells when quantifying TPD in the transiently transfected CRBN-knockout (KO) cells, we used a flow cytometer based-immunofluorescence (IF) assay. In this assay we identified CRBN-positive cells using an anti-FLAG antibody, and then used signals from anti-BRD2 and BRD4 antibodies to quantify those proteins in the CRBN-positive cells. The fraction of cells expressing CRBN was generally in the 30 - 60% range (Fig. S4). To establish the validity of the IF assay, we carried out a classic PROTAC assay using dBET6 treatment of cells transiently expressing FLAG-tagged $CRBN^{WT}$ and measured BRD2/4 levels by the IF assay (Fig. 4a). Consistent with what has been seen by others [54], the assay showed BRD2 and BRD4 degradation of 90% and 80%, respectively, and control compounds such as JQ1 by itself and its inactive (-)JQ1 isomer led to no BRD2/4 degradation. Additionally, to verify that ELF degraders had no effect on BRD2 degradation, cells expressing $CRBN^{WT}$ were exposed to 10 μM inactive C2 and PEG1 sTCO-JQ1 ELF degraders and similar effect as +JQ1 no effect was detected (S5B).

Next, we evaluated the effectiveness of the full set of six sTCO-JQ1 degraders using one target protein, BRD2, and one $CRBN^{Tet}$ form, $CRBN^{355}$. We chose residue 355 because it is right at the dBET6 binding pocket, and we hypothesized that $CRBN^{355}$ when conjugated to sTCO-JQ1 degraders would best mimic dBET6 bound to $CRBN^{WT}$ and best enable BRD2 degradation. Further controls transfected with $CRBN^{WT}$ and exposed to 0.01, 0.1 and 1.0 μM dBET1 and dBET6 all showed ~90% degradation of BRD2, and the cells containing $CRBN^{355}$ exposed to ELF degraders over the same concentration range showed a dose-dependence reduction in BRD2 for all degraders, with a maximal value of 75% degradation for the sTCO-PEG5-JQ1 degrader at 1.0 μM (Fig. 4b). Additionally, a clear trend of increased BRD2 degradation was observed with increased ELF degrader linker length. The dose dependent increase makes sense given that the ligation of the $CRBN^{Tet}$ increases with degrader concentration and only reaches completeness at 1.0 μM degrader (Fig. 3d and S3). Evidence that BRD2 degradation is induced by the proposed ELF degrader mechanism, is provided by negative controls showing that BRD2 degradation is only minimally stimulated by JQ1 itself or a degrader containing the inactive (-)JQ1 isomer (Fig. 4c). Finally, tests of degraders at a higher concentration (10 μM) resulted in much less degradation (Fig. 4c and S5), a behavior also generally observed in PROTAC studies and referred to as the "hook effect" [55-56]. The explanation for this decrease is that excess degrader (i.e. degrader not ligated to $CRBN^{Tet}$) can bind to the neosubstrate and block its binding to the degraders that are ligated to $CRBN^{Tet}$.

Given the above success with $CRBN^{355}$ and BRD2 degradation, we expanded our study of ELF degraders to monitor the degradation of both BRD2 and BRD4, and evaluate all of the initially selected six Tet sites on CRBN, five around the known IMiD-binding pocket of CRBN and one (residue 70) rather distant (Fig. 2d, 5a). Also, given the clear trends with ELF degrader length and concentration, in these further studies, we only tested the shortest and longest PEG-linked degraders (PEG1 and PEG5 respectively), and tested them only at the concentrations of 0.1 and 1.0 μM. At all six sites the ELF degraders promoted the degradation of both BRD2 and BRD4 and the dependencies on the degrader length and concentration matched those seen in the pilot studies, with the longer linker and the 1.0 μM concentration being more effective in every case (Fig. 5b,c). Even though all CRBN sites promoted degradation, the sites near the IMiD-binding pocket were much more effective, leading to a high 50-75% level of degradation of both BRD2 and BRD4, whereas site 70, far from the IMiD-binding pocket, led to just a 40% degradation of BRD2 and an even lower 20% degradation of BRD4. While this indicates that different surfaces of CRBN are differentially effective in promoting degradation, and that ELF degrader ligation of $CRBN^{70}$ promotes degradation at all indicates that there is substantial structural plasticity in how CRBN can recruit substrates.

Additional probing of the structural plasticity of CRBN promoted TPD

Given that the promotion of BRD2/4 degradation by ELF degraders was not limited to ligating CRBN residues at or near the IMiD binding pocket, we further probed the structural plasticity of CRBN function by picking four additional sites (residues 112, 259, 364 and 407) that sample the addition exposed surface areas of CRBN (Fig. 5a). Except for $CRBN^{112}$, the new CRBN forms showed Tet-ncAA dependent $CRBN^{Tet}$ expression and robust in cell labeling with 1 μM of the sTCO-PEG5-JQ1 ELF degrader (Fig. S6); for unknown reasons, $CRBN^{112}$ showed leaky expression in the absence of Tet ncAA, but a substantial fraction of the protein underwent in cell labeling with 1 μM ELF degrader, meaning it was suitable for study. Remarkably, all of these additional $CRBN^{Tet}$ forms showed a substantial ELF degrader effects, inducing 30-40% degradation of BRD2 (Fig. 5d). Interestingly, $CRBN^{112}$ and $CRBN^{70}$ which are on the same face of CRBN, both showed a slightly lower ~25% degradation of BRD2, while $CRBN^{Tet}$ sites 259, 364 and 407, which are spread out on a different face of CRBN (Fig. 5a), led to a slightly higher degradation of ~40%.

Tet-encoding is generally compatible with PROTAC function

A final question we asked is the extent to which the $CRBN^{Tet}$ protein forms can still participate in PROTAC stimulated TPD. To test this, we took the full panel of $CRBN^{Tet}$ forms and assessed the ability of dBET6 to stimulate the degradation of BRD2 and BRD4. The levels of BRD2 and BRD4 degradation achieved by $CRBN^{WT}$ were ~95% and ~75%, respectively. For both BRD2 and BRD4 none of the $CRBN^{Tet}$ forms showed substantial impairment, with all achieving degradation levels at least 80% of those stimulated by the wild-type protein (Fig. 5e). Also, the extents of impairment shown by the various forms were reasonably consistent for the two protein targets, implying that the mechanisms of impairment are the same for the two substrates. The $CRBN^{Tet}$ forms with Tet at sites 112, 259, 353 and 364 showing the most impairment for both protein targets, with the degradation being ~85% and ~60% for BRD2 and ~BRD4, respectively.

Using ELF degraders to characterize the E3 ligase SPOP

Next, we sought to apply the ELF-degrader approach to one of the many E3 ligases that have no known specific tight-binding ligand and thus have not been useful for TPD using either PROTACs or molecular glues. We chose the E3 ubiquitin ligase adaptor SPOP, a well-studied E3 from the cullin ring ligase family that naturally recognizes a degron present in bromodomain and extraterminal (BET) family proteins including the proteins BRD2 and BRD4[57-59]. SPOP has three domains (Fig. 7a), a MATH domain for degron binding, and BTB and BACK domains involved in forming the CRL3 complex and higher level assemblies (Fig. S7)[60 61].

Since wild-type SPOP naturally targets BRD2/4 for degradation, it provides a stringent test of whether the ELF-degraders can target even more degradation of BRD2/4 compared to that accomplished by wild type SPOP. To select sites for Tet incorporation, we carried out a standard computational analysis [62] to identify "druggable" surface regions, and of the top two identified sites, only one, a region near Asn40 at the edge of a beta sheet and Glu78 on a flexible loop were well-exposed in the CRL3 complex (Fig. 7b and S7b). Based on this we chose Asn40 and Glu 78 plus three additional sites distributed on exposed surfaces of the MATH domain: Glu78 on a flexible loop somewhat near the druggable site, Trp131 and Arg121 at and near the degron-binding loop, and Ser55 on a surface distant from the other sites (Fig. S7b).

Using the same GCE system as above, but with FLAG-tagged SPOP genes in the place of CRBN genes (Fig. 7a), the five SPOP mutants encoding Tet3Bu and a wild-type SPOP control were transiently expressed in standard HEK293T cells. All of the SPOP forms expressed well and the Tet3Bu-containing forms ($SPOP^{Tet}$) when released from the cell were fully reactive with sTCO-PEG_{5K} (Fig. S8a). We also found the proteins appeared as doublet on a gel, and consistent with reports that such doublets were due to phosphorylation[63-64], we found that a λ phosphatase treatment led to the disappearance of upper band (Fig. S8b).

To test if the IF assay could work in the presence of transiently expressed SPOP, we carried out a set of control assays for BRD2 degradation in standard HEK293Tcells without or with wild-type SPOP ($SPOP^{WT}$) expression (Fig. 7c). The purpose of the dBET6 control was to leverage its interaction with the endogenous CRBN to induce BRD2 degradation, and in that way demonstrate the maximum achievable extent of BRD2 degradation. This result establishes two things: first that $SPOP^{WT}$ expression, as expected, leads to lower BRD2 levels since it is a natural BRD2 degrader (Fig 7c, raw data), and second that even with the reduced BRD2 levels seen after $SPOP^{WT}$ expression, further degradation of BRD2 is possible. Thus the system is suitable for assessing the ability of an SPOP-ligated ELF-degrader to mediate additional degradation.

To our surprise, in the additional controls with 1 μM of (+)JQ1, (-)JQ1 or the sTCO-PEG5-JQ1 ELF degrader, the residual BRD2 was reduced – by 20, 25% and 75%, respectively – even though $SPOP^{WT}$ cannot covalently react with any of them (Fig. 7c). We speculated that this additional degradation was due to a nonspecific effect in which these rather nonpolar molecules enhance the $SPOP^{WT}$:BRD2 degron interaction. Consistent with this, we showed that a much lower 10 nM concentration of the sTCO-PEG5-JQ1 ELF degrader, caused additional BRD2 degradation of less than 10% (Fig. 7c), establishing this as a concentration that could be used for evaluating $SPOP^{Tet}$ directed degradation.

Next, we tested $SPOP^{WT}$ in parallel with the five $SPOP^{Tet}$ variants in HEK293T cells using 10 nM sTCO-PEG5-JQ1 ELF degrader for the ligations and assessing BRD2 levels (Fig 7d). As

was seen above, $SPOP^{WT}$ expression decreased residual BRD2 levels (Fig 7d, raw data) and in the presence of 10 nM sTCO-PEG5-JQ1 degrader there was only a minimal ~10% increase in degradation. We further found that, in the absence of ligation, the site-specific encoding of Tet ncAAs into SPOP had little effect on the degradation of BRD2, except for the $SPOP^{131}$ variant, which showed substantially more residual BRD2. In fact, the BRD2 levels for this variant were roughly equal to that of non-transfected cells (Fig 7d raw data), implying that SPOP with a Tet3Bu side chain at position 131 no longer recognized the BRD2 degron. This result is consistent with reports that this side chain is at the degron binding site and is critical for BRD2 binding[59]. In contrast, when treated with 10 nM sTCO-JQ1 PEG5 degrader all five $SPOP^{Tet}$ forms showed a significant loss of BRD2 (Fig 7d). A 50-70% loss of BRD2 signal was observed for $SPOP^{Tet}$ at sites 78, 121 and 131, while a more modest ~30% loss of BRD2 was observed for Tet3Bu at sites 40 and 55.

Noticing the advantage provided by the inability of the $SPOP^{131}$ variant to degrade BRD2, we modified our expression system to replace $SPOP^{WT}$ with a W131A-SPOP mutant, a mutant known to have much reduced degron binding[59]. We hypothesized that W131A-SPOP variants with or without Tet incorporated would not themselves contribute to BRD2 degradation, and the higher levels of residual BRD2 in the cells would allow for greater sensitivity in measuring BRD2 degradation after ligation with an sTCO-JQ1 ELF degrader. The IF assay results show that expressed W131A-SPOP does indeed lead to higher BRD2 levels in the cell, and these levels are even higher, by about 40%, than are seen in untreated HEK293T cells (Fig 7e). We do not know the origin of this effect, but suspect it could be related to the oligomeric nature of the CUL3-SPOP assembly (Figure S7a) which makes it possible that a mixing of inactive SPOP chains with the endogenous SPOP negatively impacts the function of the assembly. Alongside this result, the dBET6 positive control shows a very large decrease of BRD2 signal showing that the BRD2 present is available for degradation, and the addition of 10 nM ELF-degrader shows no effect on BRD2 levels.

Turning to the W131A-SPOP variants with Tet encoded at sites 40, 55, 78, and 121, we see that in the absence of added ELF-degrader the expression of each of those proteins also leaves BRD2 levels that are higher than the untreated HEK293T cells (Fig 7e), although they vary substantially, possibly due to differential levels of expression leading to differential impacts on the CUL3-SPOP assembly. Upon ligation of these W131A $SPOP^{Tet}$ variants with 10 nM of sTCO-PEG5-JQ1 ELF-degrader, all show enhanced BRD2 degradation, with the decrease in BRD2 varying from ~10-15% for sites 40 and 55, and ~50% and ~60% for sites 121 and 78, respectively.

DISCUSSION

The discovery that TPD could be accomplished by repurposing the cell's UPS has revolutionized therapeutic strategies by providing access to the massive intracellular undruggable proteome [65]. However, even though many PROTAC and "molecular glue" therapeutics have been developed, the huge potential for application to degrade specific, disease-causing target proteins has been limited due to the small number of E3 ligases [33-35] for which high-affinity ligands are known [36-37]. Indeed, even while computational methods can identify potential sites for ligand development on novel E3 ligases, no methods exist to evaluate whether a PROTAC-like molecule binding at the putative ligand site would also have a geometry that could drive target protein ubiquitination and subsequent degradation. It is to address this gap in knowledge that we sought here to develop an E3 ligase ligand free degrader

(ELF-degrader) that in live cells can be site-specifically positioned on any E3 ligase to map the surface of E3 ligase and identify optimal pockets for TPD.

ELF-Degrader Strategy

Genetic code expansion (GCE) technology offers a powerful tool for a minimally-perturbing site-specific incorporation of new chemical functionality into proteins in live cells, and this enables protein interactions to be studied in their native cellular environment. While GCE has been used to covalently identify interacting proteins with photo-reactive ncAAs and evaluate protein dynamics in cellular processes [44, 66-67], encoding bioorthogonal chemistry was selected to provide high labeling efficiencies in short times [47, 68-70]. While many GCE encoded chemistries have enabled antibody functionalization to form antibody-drug conjugates, few have the labeling efficiency or speed to quantitatively label proteins for functional alteration inside live cells. Here, we choose to encode tetrazine amino acids on the E3 ligase surface because this approach has the fastest stoichiometric in-cell labeling rates with sTCO functionalized ligands[71,72] and offers quantitative labeling of E3 target proteins at low cellular concentration of protein and ELF-degrader. We selected the CRBN E3 ligase to identify the limits of the ELF-degrader system, since Tet-ncAAs encoded near the IMiD-binding pocket could be labeled with sTCO functionalized with a JQ1 moiety in a way that should mimic CRBN bound to dBET6 – a potent and selective degrader that comprises JQ1 conjugated to the CRBN specific binder pomalidomide. These CRBN-JQ1 conjugates would then bring the targeted BRD domain in proximity with the ubiquitin ligase complex, leading to efficient ubiquitination and proteasomal degradation. By altering the surface locations of the Tet-ncAA and the nature of the linker composition of sTCO-JQ1 degrader molecules (Fig. 2), we can monitor cellular levels of BRD2 and BRD4 and optimize ELF-degrader conditions.

Establishing the ELF-Degrader System

First, we picked five sites (Fig. 2d) around the IMiD-binding pocket to encode Tet3Bu and along with one control site (residue 70) far from predicted protein interactions and the IMiD-binding pocket. For all sites we demonstrated complete Tet3Bu encoding and their ability to label quantitively in HEK293T CRBN K/O cells confirming the robustness of this GCE approach (Fig 3). Next we confirmed that all the sTCO-JQ1 degraders with varying linker composition could enter cells and quantitatively label the $CRBN^{Tet}$ (Fig 3d). This ability allowed us to proceed with evaluating a variety of CRBN surface attachment sites and degrader linker lengths in terms of how well the resulting CRBN-JQ1 conjugates degraded protein targets directly in live cells.

To monitor TPD, we developed an IF staining assay which specifically monitors the cellular level of the BRD2/4 target proteins in E3 ligase producing cells and validated the assay by demonstrating 75-95% loss of BRD2/4 levels in the presence of dBET1 and dBET6, while control compounds such as JQ1 by itself and its inactive (-)JQ1 isomer led to no BRD2/4 degradation (Fig 4 a,b). To evaluate the effectiveness of the six sTCO-JQ1 degraders at low concentrations (0.01 to 1.0 μM), we monitored the loss of BRD2 with cells containing $CRBN^{355}$, a variant placing the Tet-ncAA right at the edge of the dBET6 binding pocket (Fig 4b). This clearly demonstrated that ELF degraders did work, as at the optimal degrader concentration of 1 μM and with the longest of the linkers (PEG5), the cellular BRD2 was reduced by 75%. Minimal degradation of BRD2 occurred when cells are exposed to JQ1 itself or a degrader containing the inactive (-) JQ1 isomer (Fig. 4c), supporting our proposed ELF degrader mechanism. As expected, substantially less target degradation was detected at a

higher 10 μM degrader concentration, a behavior referred to as the "hook effect" in PROTAC studies[55-56]. A primary reason for selecting a GCE labeling system with fast intracellular labeling rates was to enable avoiding the "hook effect" by using low label concentrations such that the ligation could proceed in a reasonable timeframe, even while having a minimal excess of unreacted label.

Site-Specific Degradation Efficiency and Plasticity of CRBN

This validation of ELF degrader function encouraged us to evaluate the robustness of this approach for removing BRD2 and BRD4 using the four other $CRBN^{Tet}$ sites around the IMiD-binding pocket and the $CRBN^{70}$ site far from IMiD-binding pocket (Fig 2d, 5a). Impressively all sites near the IMiD-binding pocket, after reaction with an ELF degrader, showed 50-75% degradation of both targets when the longer PEG5 linker was used and slightly less degradation with the shorter PEG1 linker (Fig 5b,c). And interestingly, these five sites led to nearly equivalent (within ~5% of each other) degradation levels of BRD2 and BRD4. In contrast, ligation at the distant $CRBN^{70}$ site promoted degradation to a lesser extent, degrading ~40% of BRD4 and ~20% of BRD2. This is an important result, because it indicates that there is substantial structural plasticity in how CRBN can recruit targets, while also making clear that surface site location can lead to functional preferences that differentially impact different target proteins.

To further evaluate the structural plasticity of CRBN with ELF degraders, we tested four additional sites that sample additional exposed surfaces of CRBN. We discovered that the two sites (70 and 112) on the same face but far from the IMiD-binding pocket had similarly low BRD2 degradation ability (10-25%) whereas the three $CRBN^{Tet}$ sites 259, 364 and 407, on the opposite face showed improved (25-40%) degradation ability (Fig. 5b, d). This ability to "walk" the ELF degrader position around the surface of E3 ligases with site-specific control in order to probe functional constraints and potential ligand binding pockets reveals how the ELF degrader approach is a powerful tool that makes it possible to efficiently explore the therapeutic potential of E3 ligases for which ligands have not been identified.

Our final experiment was motivated by the realization that even though Tet-ncAA encoding on an E3 ligase is a small structural change, it could still compromise protein conformation or stability and negatively impact CRL4-complex formation or dBET6 binding and thus functions. Since all $CRBN^{Tet}$ forms enabled BRD2/4 degradation at levels on par with those stimulated by $CRBN^{WT}$ (Fig 5e), we conclude that Tet-modified E3 ligase forms will, in general, be compatible with PROTAC function. Interestingly, of the four most impaired sites, only one (residue 353) was at the PROTAC binding site where it is easy to understand how the mutation could impact PROTAC binding. The other three (residues 112, 259 and 364) were at surface positions rather distant from the PROTAC binding site (Fig. 5a), implying that the mutations at these sites are somehow impacting the assembly or functionality of the CRL4-complex.

Modeling ELF Geometry and Mechanism of Action

A modeling of open and closed CRL4-complexes with ELF degraders attached at different $CRBN^{Tet}$ surface positions (Fig. 6) shows how the ELF degrader results are consistent with a simple distance model for how the site of attachment alters the extent of target protein degradation. The $CRBN^{355}$ position modified with the longest (the PEG5) ELF degrader and bound to BRD4 shows a very short distance for ubiquitin transfer for both the open and closed

complex forms. Alternatively, CRBN[70] when bound to BRD4 has a much longer distance for ubiquitin transfer in both open and closed forms. And the degradation data correlates well with distance, as attachment sites around the IMiD-binding pocket produce the highest degradation levels, sites with the longest distances (70 and 112) show the lowest degradation levels, and sites with a middle distance (359, 364, and 407) provide a medium degradation level. This modeling also shows that the conformational shift from open to closed CRBN forms does impact the geometry for ubiquitination (Fig. 6a versus b)[73]. Notably, since ELF degrader ligation would not be expected to trigger the conformational change, the lack of such a change could be a factor in why none of the $CRBN^{Tet}$ forms ligated with ELF degraders achieved the same level of BRD2 degradation as promoted by dBET1 or dBET6.

Application of ELF-Degraders to SPOP

We have demonstrated that our ELF degrader approach can be applied to other E3 ligases and importantly to those with no known ligand binding site. The $SPOP^{Tet}$ expression and labeling data showed that it has a similar propensity to label with ELF degraders. And the IF assay data show that even a very low 10 nM concentration of ELF degrader is sufficient to promote the degradation of the BRD2 target protein that drives BRD2 levels to even lower levels than are achieved by SPOP degrading BRD2 through recognition of its natural degron. Also, the results with SPOP reinforce what we observed for CRBN, that it is possible to promote targeted protein degradation by ELF-degrader ligation at sites that are at widely differing places on the protein surface. Our computational predictions for druggable binding sites on SPOP combined with the ELF-degrader degradation results – specifically the ~65% degradation achieved with the ligation at site 78 – identifies this surface of the protein as an attractive one to pursue for ligand design, and more generally establishes that there can be druggable binding locations on an E3 ligase that will promote TPD even though they are far from the degron binding site (Fig. 8). Additionally, the strong degradation profile for ELF degraders on SPOP at the degron recognition site, $SPOP^{131}$ and near this site, $SPOP^{121}$ (Fig. 7d) implies that developing a molecular glue at or near this interface would boost the native degradation process.

Conclusion and Future Directions for ELF-Degraders in TPD Discovery

In summary, we demonstrate that the site-specific encoding of Tet-ncAAs can be used to rapidly functionalize E3-ligases in live cells with protein-targeted degrader ligands and that this robust system can be used to evaluate the structural organization of the UPS.

While completing our study, other groups reported complementary site-specific GCE approaches, also done in live cells, which involve attaching E3-ligase recruiting ligands onto target proteins to promote TPD of target proteins[74-75]. This highlights the versatility of ways that such GCE-enabled approaches can advance the TPD field. Additionally, given the broad orthogonality of the GCE systems used, the ELF-degrader approach can be implemented in a wide variety of eukaryotic cell types [76-77]. The design of the ELF-degrader approach enables it to be applied to any E3 ligases for exploring not only their potential for neo-substrate TPD, but also to specifically explore those sites on their surfaces that are computationally identified as attractive sites for ligand development. Furthermore, since we showed this GCE bioconjugation approach of encoding Tet-ncAA on CRBN is compatible with traditional PROTAC function, this work also opens the door to using on-protein Tet ligation to attach a fluorescent probe to functional E3 ligases and track changes in complexation and sub-cellular localization under native states and in response to PROTAC treatment.

METHODS

Plasmids. All the plasmids used for the experiments have been summarized in Table SI-1. The synthetase plasmid was pAcBac1-R2-84-RS, pAcBac1-sfGFP-^{150TAG} (Plasmid Control for Tet expression having C-term FLAG tag), pAcBac1-sfGFP-^{WT} (transfection control plasmid), Gene of interest (GOI) plasmids were pAcBac1-CRBN^{WT} (N-term FLAG tag), pAcBac1-CRBN^{TAG}s , pAcBac1-SPOP^{WT} (N-term FLAG tag), and pAcBac1-SPOP^{TAG}s (Table SI-1).

Transfection of HEK cells. HEK293T, and HEK293T CRBN K/O cells were grown in DMEM /10% FBS (Fetal Bovine Serum). The cells were plated in a 24-well plate at 1:3 ratios from the 100 % confluent plate so that they reach 70% to 80% confluency at the time of transfection. Cells were transiently transfected using JetPrime (*Polyplus-transfection*®) using the manufacturer's protocol with minor modification. Briefly, 600-800 ng of plasmid DNA was taken in 1:8 [RS: GOI], 50 µl of JetPrime Buffer, and 1.2 µl of JetPrime reagent. They were combined and incubated for 20 min at RT before adding to cells. Tet3Bu amino acid at 30 µM was added to the cells immediately and incubated for 24-48 h, depending on the experiment, before analysis. For SPOP, Briefly, 400-500 ng of plasmid DNA was taken in 1:8 [RS: GOI], 75 µl of JetPrime Buffer, and 2.4 µl of JetPrime reagent with Tet3Bu amino acid at 5 µM incubated for 24-48 h.

***In-Vivo* Tetrazine labeling and mobility shift assay:** To examine the specific *in-cell* labeling of CRBN^{Tet} and SPOP^{Tet} proteins in HEK293T cells, transfected cells were washed two times with DMEM media and incubated for 1 or 6 h with 1,10 and 0.1-10 µM sTCO-JQ1 degraders respectively. Unreacted degraders were quenched by at least three molar excess of Tet2-Me [53]. Cells were washed with PBS and lysed using RIPA lysis buffer system (Santa Cruz Biotechnology, sc-24948). To the cell lysate, 20µM of sTCO-PEG$_{5K}$ was added for 15 min and then quenched with Tet-v2.0Me for 5 min. The samples were then prepared using β-mercaptoethanol Laemmli buffer and after thermal denaturation, the lysates were separated by 12% SDS-PAGE followed by transfer to nitrocellulose membranes.
The membranes were blocked with Licor Blocking buffer for 60 min and then washed three times with TBS-T (tris-buffered saline containing 0.1% Tween-20), incubated with a primary (Mouse AntiFLAGM2) antibody for 60 min, washed three times with TBS-T and then incubated for 60 min with a secondary (Anti Mouse 680IR) antibody followed by washing again three times with TBS-T before imaging. Immunoreactive bands were detected Licor Instrument.

The immunofluorescence (IF) assay for assessing CRBN-mediated degradation of target protein (BRD2/4): HEK293T or CRBN-K/O cells were transfected with 800 ng of CRBN^{WT} or CRBN^{Tet}-expressing plasmid DNA, and grown for at 36 – 48 h, with 30 µM Tet3Bu in the case of CRBN^{Tet}-expressing cells. For SPOP expressions plasmid DNA was reduced to 400 ng and Tet3Bu was reduced to 5 µM to limit SPOP intracellular concentration. Cells then underwent treatment for 6 h with a TPD agent (either dBET6, dBET1 or an ELF degrader) or a control compound. While more complete TPD may be achieved by ELF degraders at longer incubation times, longer times were not used to minimize degradation artifacts leading from global transcriptional changes[78-79]. After treatment, cells were prepared using BD cytofix/cytoperm fixation/permeabilization kit (BD Biosciences) according to the manufacturer's instructions. Cells were first stained with FLAG primary antibody (Sigma F1804, 1to200 dilution), and then stained for BRD2 (Abcam ab197865, 1to50 dilution), anti-mouse IgG (Thermofisher A-32742, 1to200), and BRD4 (Abcam ab197608, 1to50). All staining procedures were performed for 30 min at 4 °C. Samples were analyzed on an LSR

Fortessa X-20 (BD Biosciences), and data were processed using FlowJo (v.10.10),0) analysis software (BD Biosciences). FLAG-positive singlets were manually gated, and the population median fluorescent intensity (MFI) and median absolute deviation (MAD) were extracted from each condition for visualization. In every acquisition at least 1000 cells were collected in the final FLAG + population, it's the variation within the cell population.

Figures

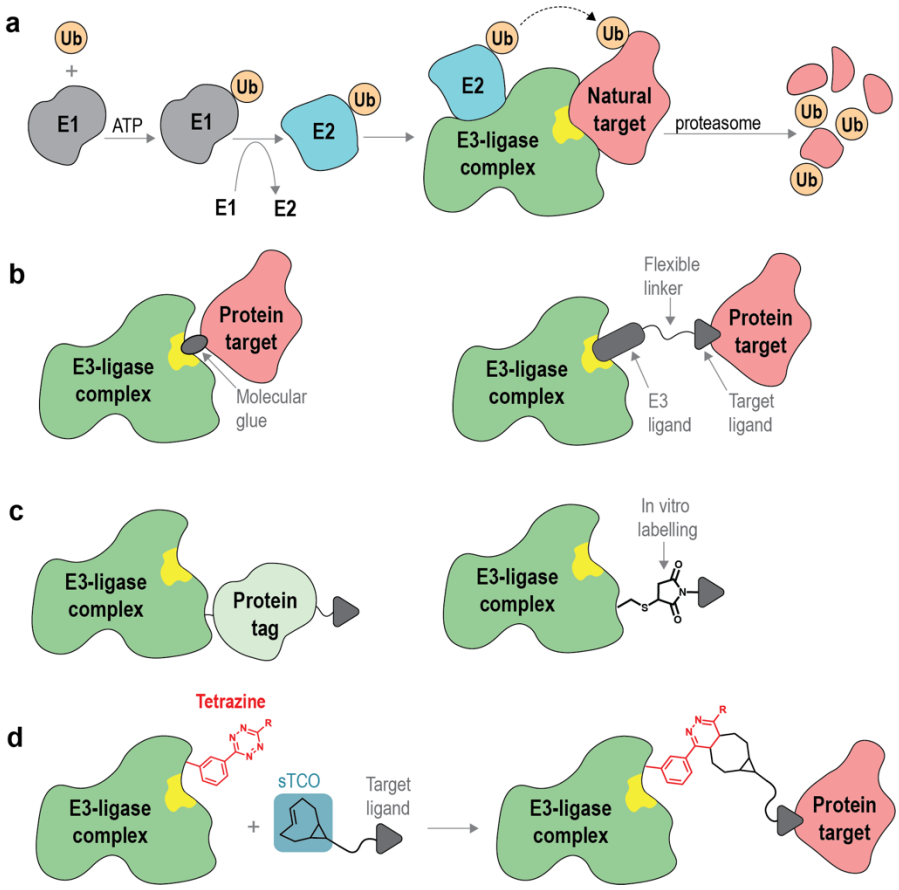

Fig. 1: Strategies for targeted protein degradation. (a) Steps in the natural Ubiquitin Protease System (UPS) highlighting the role of the E3 ligase complex (green), putative binding site (yellow) in recognizing the target protein (pink) that is destined for ubiquitination and degradation. (b) How a molecular glue (left) and bi-functional PROTAC molecule (right) bring an E3 ligase and a neosubstrate target protein into proximity and triggering its ubiquitination and degradation. (c) Current approaches to study TPD using protein fusion tags (left) and *in vitro* label conjugation followed by electroporation into cells (right) (d) Concept for how an E3-ligand free (ELF) degrader (consisting of a trans-cyclooctene group linked to a target protein ligand), after a click chemistry reaction with an E3 ligase containing a tetrazine moiety, can mimic the functionality of a PROTAC molecule in bringing an E3 ligase and target protein together independent of the binding site.

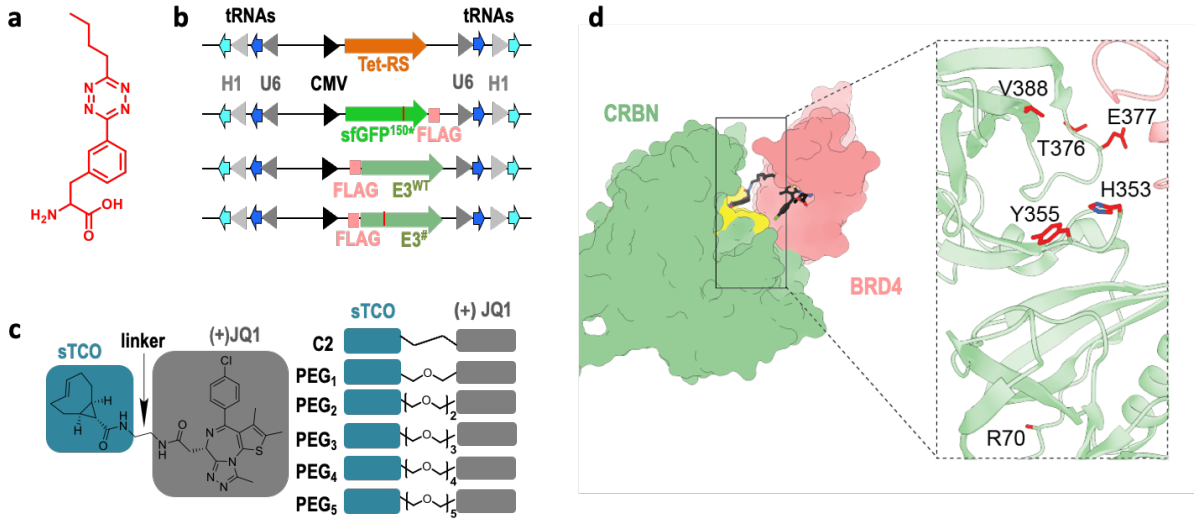

Fig. 2: Components used in developing the ELF degrader approach. (a) Chemical structure of the tetrazine3.0-butyl (Tet3Bu) ncAA, shown in red throughout this paper. (b) Plasmid constructs with GCE machinery (NES-RS and tRNAs), control sfGFP^{150}, and protein of interest (CRBN) genes with FLAG-tags as shown and promoters. Also noted are cytomegalovirus (CMV), and H1 and U6 tRNA promoters. (c) Chimeric ELF degrader reagents all have strained trans-cyclooctene (blue box) at one end and a JQ1 target protein ligand (grey box) at the other. Right-hand part names and shows the seven linkers used. (d) Space-filling image of the complex between Cereblon (green with yellow iMiD binding pocket), BRD4 (pink) and the bifunctional PROTAC dBET6 (black sticks), (PDB code: 6BN7, R70 density was not modeled)[51]. Close up of interface shows ribbon diagram highlighting the six CRBN residues (red stick models) initially selected for tetrazine incorporation.

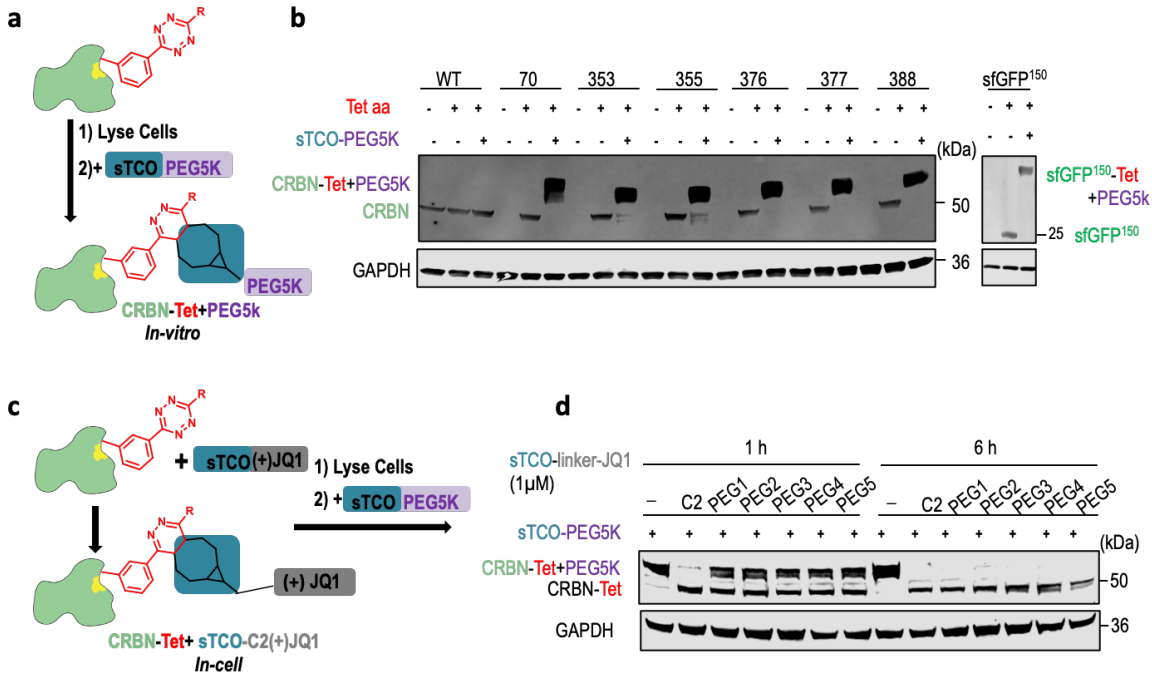

Fig. 3: Expression and ligation of CRBN^{Tet} forms in mammalian cells. (a) Design of mobility shift assay for the *in vitro* reactivity of expressed CRBN^{Tet} forms with sTCO-compounds. (b) Annotated FLAG-tag-based immunoblot for CRBN variants (left hand gel) and sfGFP150 control (right hand gel) documenting expression levels in HEK293T cells and reactivity based on mobility shift after *in vitro* reaction with sTCO-PEG$_{5K}$. GAPDH loading level control included. (c) Design of mobility shift assay for the *in vivo* reactivity of CRBN^{Tet} forms with sTCO-JQ1 degraders. (d) Annotated immunoblot, as in Panel b, of mobility shift assay to detect residual reactivity of CRBN^{355} after *in vivo* reaction for either 1 or 6 h with 1 μM of each of the six sTCO-JQ1 ELF degraders.

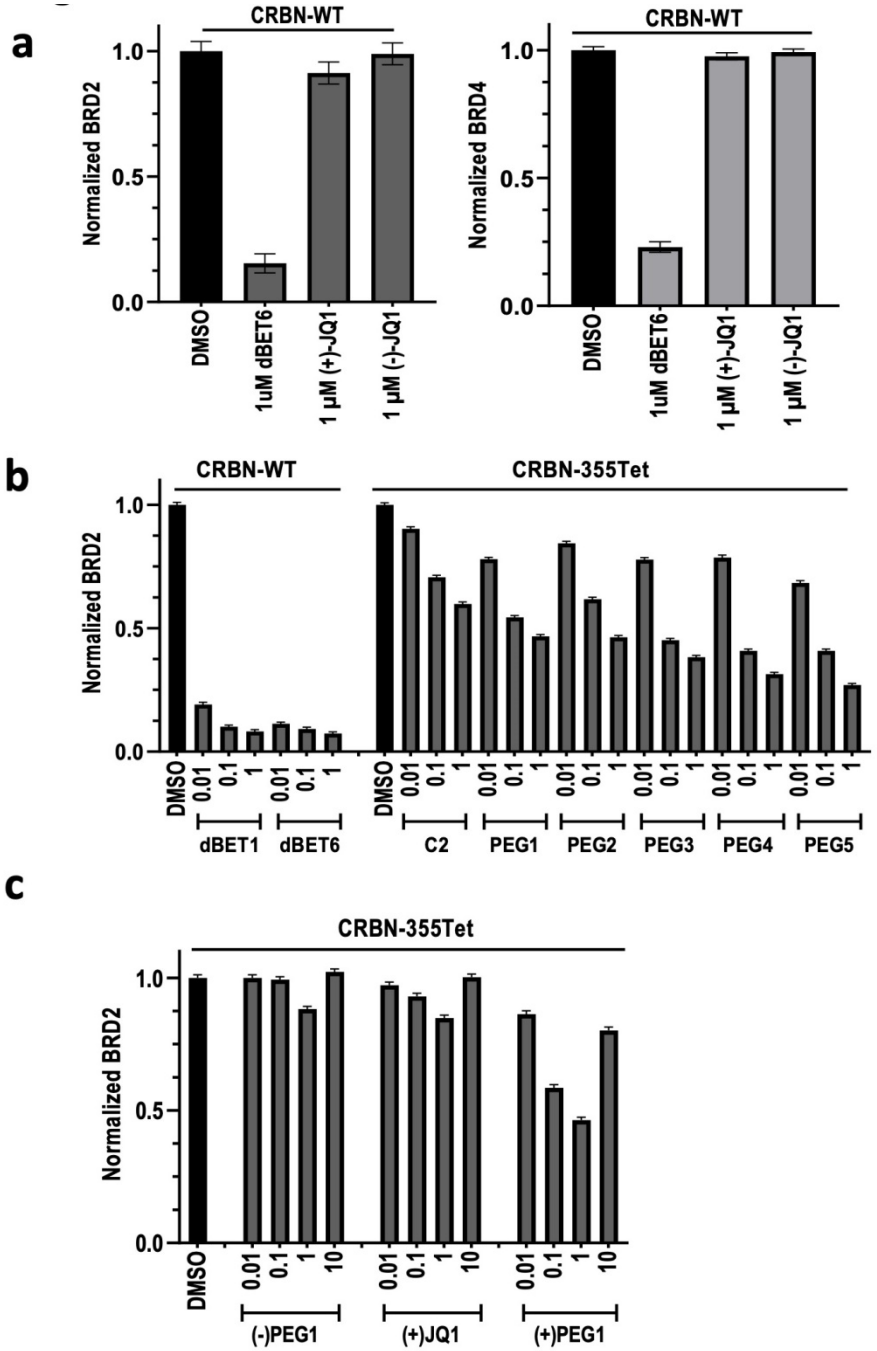

Fig. 4: Ligation of CRBN^{355} with ELF degraders promotes dose-dependent degradation of BRD2. All panels show the fraction of remaining target protein (BRD2 or BRD4) as a function of treatment, noted on the x-axis. All IF assays were carried out using HEK293T CRBN K/O cells transfected with 800 ng CRBN^{WT} or CRBN^{355} plasmid and grown at least 36 h. (a) Cells expressing CRBN^{WT} were treated with 1 µM of dBET6, active (+)JQ1, or inactive (-)JQ1 for 6 h before assaying. (b) CRBN^{WT} control results (left hand conditions) are shown with CRBN^{355} results from cells grown with 30 µM Tet3Bu then treated for 6 h with 0.01, 0.1, 1 µM of sTCO-JQ1 ELF degraders. The data shown here is representative of other sites. (c) CRBN^{355} negative controls using (-) PEG1 (a degrader with the inactive (-) JQ1 isomer) and JQ1 alone. Also included are CRBN^{355} results using the PEG1 degrader at 0.01, 0.1, 1 and 10 µM.

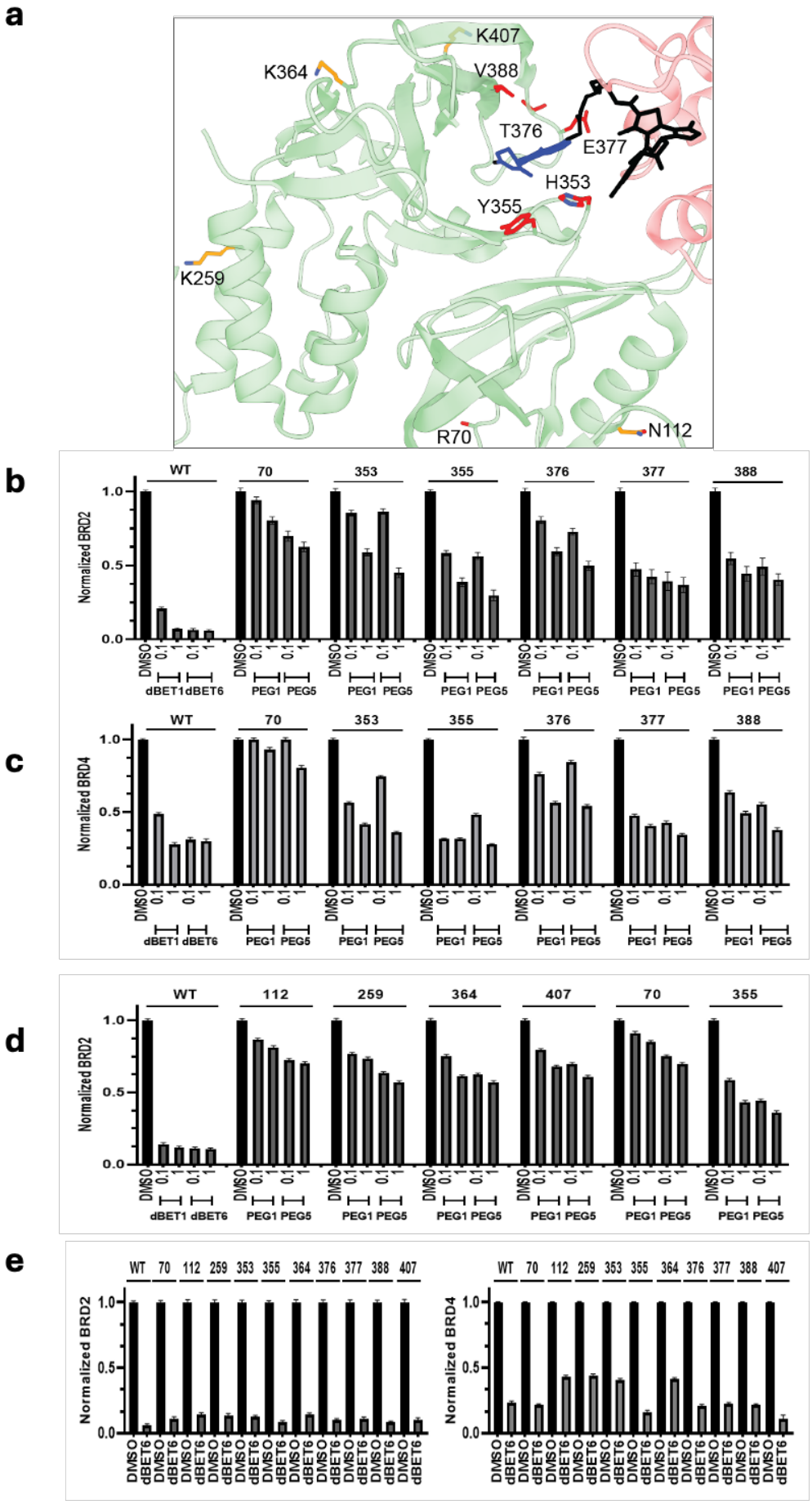
a
K407
K364
V388
T376
E377
H353
Y355
K259
R70
N112
b
WT
70
353
355
376
377
388
Normalized BRD2
1.0
0.5
0.0
DMSO
0.1
1
dBET1
dBET6
PEG1
PEG5
c
Normalized BRD4
d
112
259
364
407
e

Fig. 5: ELF degrader effectiveness varies as a function of the CRBN surface position. IF assay result plots are as in Fig. 4. (a) Ribbon diagram of CRBN: BRD4 complex as in Figure 2d, but showing side chains (red sticks with residue numbers) for the six originally targeted Tet sites and the four additional sites covering surface area of CRBN in yellow sticks (N112, K259, K364, K407). (b) BRD2 degradation results for original $CRBN^{Tet}$ target sites using 0.1 and 1 μM concentrations of the PEG1 and PEG5 ELF degraders. Positive $CRBN^{WT}$ controls with dBET1 and dBET6 and a negative DMSO solvent control are included. (c) Same as Panel b, but for BRD4 degradation. (d) Same as Panel b, but for four additional CRBN surface sites (112, 259, 364, 407) shown in Panel a. (e) IF results for BRD2 (left-hand plot) and BRD4 (right-hand plot) degradation promoted by 1 μM dBET6 treatment of each of the 10 $CRBN^{Tet}$ forms.

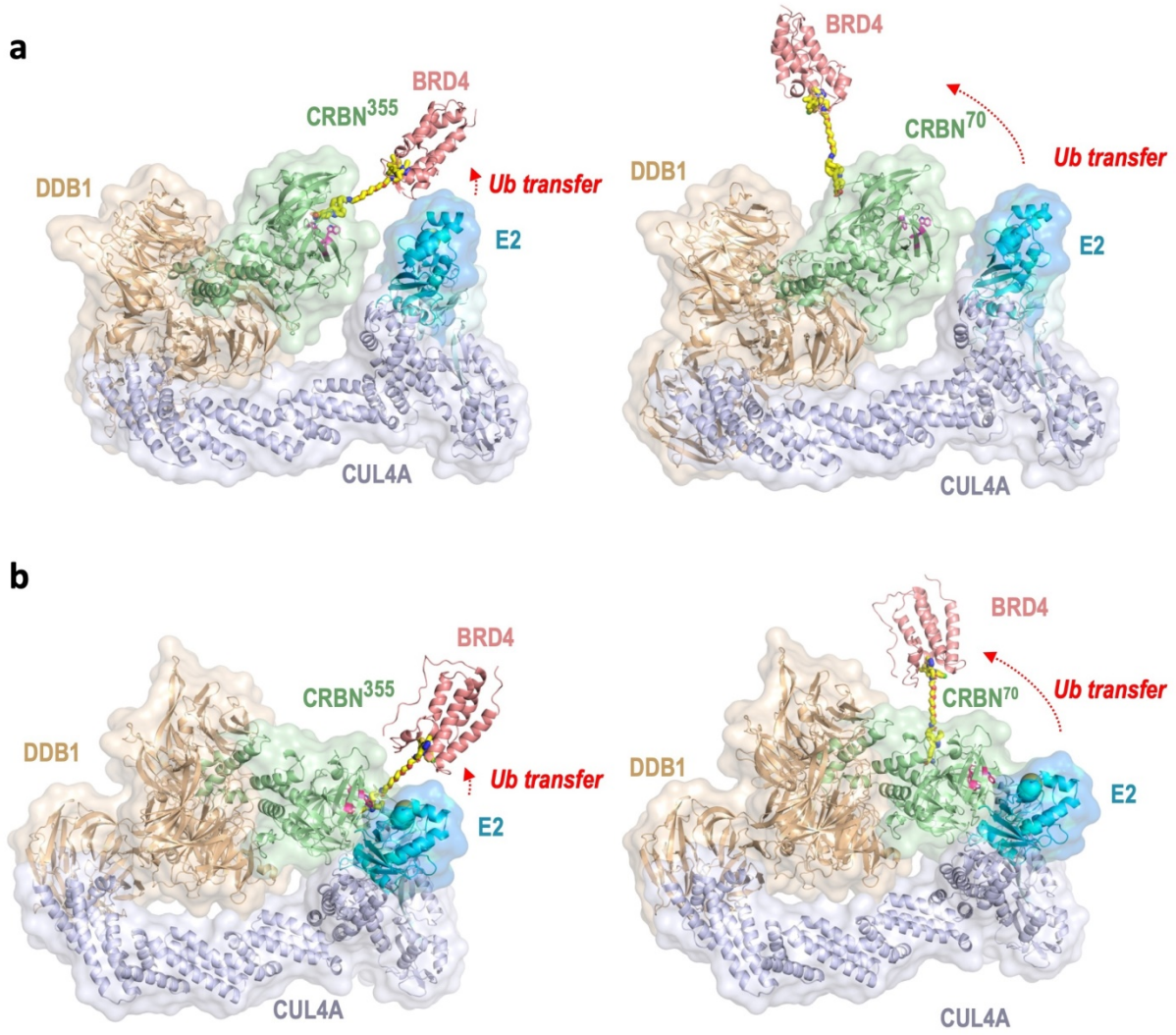

Fig. 6: Modeling supports a distance-based explanation for ELF degrader effectiveness. (a) The open conformation of a CRL4 complex including CRBN and BRD4 is shown, with the BRD4 molecule moved to be placed at the end of a modeled PEG5 linker attached at residue 355 (left hand panel) or 70 (right-hand panel). Transparent surfaces and ribbon diagrams for each protein (colored as in Fig. 1b) are labeled and the distance over which ubiquitin must be transferred is highlighted (red text and arrow). (b) Same as Panel a but based on the closed conformation of a CRL4 complex including CRBN and BRD4. The core model consisting of E2 (UBE2G1, uniprot no. P62253), RBX1 (uniprot no. P62877), CUL4A (uniprot no. Q13619) and the BPB domain of DDB1 (residues 393-709, uniprot no. Q16531) were generated using AlphaFold3 [80]. The open and closed conformations were generated by overlaying the DDB1 BPB domains from the twisted (PDB 2HYE,[81]) and hinged (PDB 5HXB,[82]) CRBN/DDBP1 structures onto the DDB1 BPB domain of the AlphaFold3 generated core structure, respectively. The JQ1 moiety of the sTCO -JQ1-PEG5 ELF degrader (generated using Phenix Elbow,[83]) was docked into BRD4 by overlaying it with the same moiety of the BRD4/JQ1 co-complex structure (PDB 3MXF,[84]).

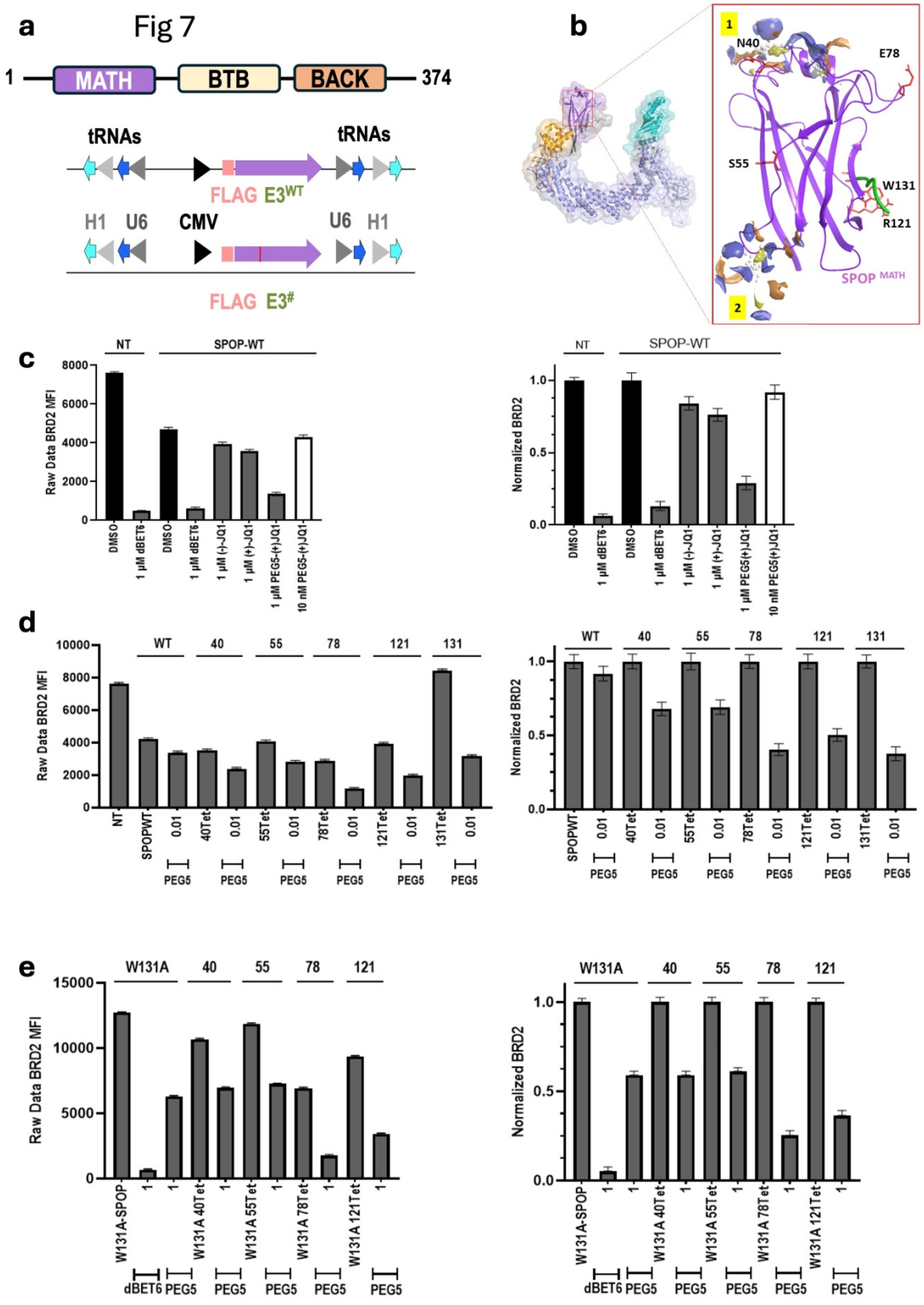

Fig 7: ELF degrader effectiveness on the E3 ligase SPOP. (a) SPOP-monomer domain architecture and GCE plasmids, annotated as in Fig. 2b, for expressing FLAG-tagged SPOP^{WT} and SPOP^{Tet} variants. (b) Ribbon diagram of modelled SPOP:CRL3 complex, with a close up of the SPOP MATH domain (purple) including a bound BRD3 degron (green), two potentially ligandable sites (numbers 1 and 2) identified by SiteMap[62] (for surface colors see Fig. S7b),

and the five tetrazine incorporation sites across the SPOP surface (red stick models with residue numbers). (c) IF assay BRD2 degradation results (shown as in Fig. 4) for positive and negative controls to establish suitable conditions for experiments with transiently expressed SPOP in HEK293T cells. Results are shown both before (left side) and after (right side) independently normalizing the results for each site. (d) As Panel c, but for $SPOP^{Tet}$ forms ligated with 10 nM PEG5 ELF degrader. (e) As Panel d, but for four $SPOP^{Tet}$ variants in the context of a W131A mutation.

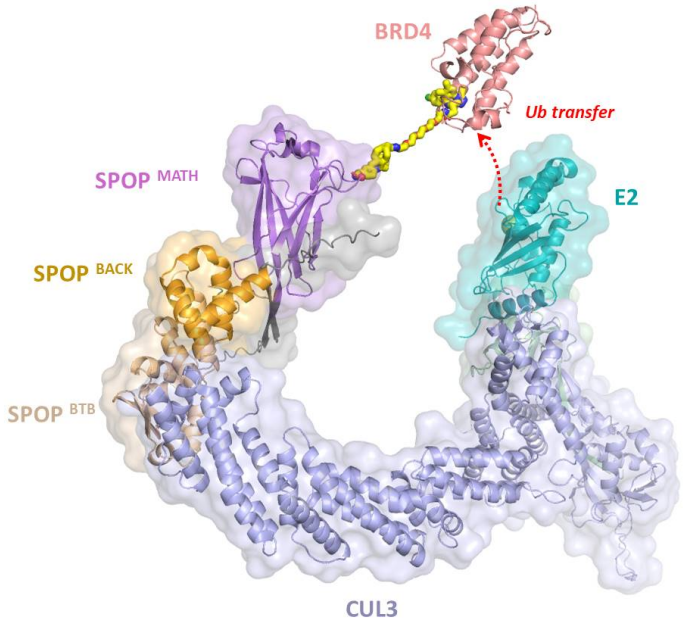

Fig 8: **Computational Modeling of Druggable SPOP Binding Sites Distant from the Degron Interface.** Alphafold3 generated molecular model of the CUL3-SPOP monomer including UBE2G1 E2 ligase (cyan, uniprot no. P62253), RBX1 (light green, uniprot no. P62877), CUL3 (blue, uniprot no. Q13618), and SPOP (as colored in panel A, uniprot no. O43791) with a BRD4 molecule (pink, PDB 3MXF) at the end of a modeled PEG5 linker (yellow) attached at residue E78 of SPOP. Transparent surfaces and ribbon diagrams for each protein are labeled and the distance over which ubiquitin must be transferred is highlighted (red text and arrow). The JQ1 moiety of the sTCO -JQ1-PEG5 ELF degrader was generated and docked into BRD4 as in Fig. 6.

Supporting Information
The Supporting Information includes supplemental methods (S1-S8, figures S9-S14, supplemental tables S15, ^{1}H AND ^{13}C NMR spectra S16-S31 and references S32).

Acknowledgments
We are grateful for the assistance from Jeff Moore for mass spectrometry data acquisition and processing.

Funding
This work was supported in part by the GCE4All Biomedical Technology Development and Dissemination Center supported by National Institute of General Medical Science grant RM1-GM144227 and 1S10RR025628-01 to the Oregon State University Mass Spectrometry Facility.

COMPETING INTERESTS
The authors declare the following competing financial interest(s): Y.Z., Z.N., V.M., J.Y., K.P., S.W., A.V., J.M.R. are current employees of AbbVie. P.R. was an employee of AbbVie at the time of the study. The design, study conduct, and financial support for this research were provided in part by AbbVie. AbbVie participated in the interpretation of data, review, and approval of the publication.

References

(1) Koga, H.; Kaushik, S.; Cuervo, A. M., Protein homeostasis and aging: The importance of exquisite quality control. *Ageing research reviews* **2011,** *10* (2), 205-215.
(2) Powers, E. T.; Gierasch, L. M., The proteome folding problem and cellular proteostasis. *Journal of molecular biology* **2021,** *433* (20), 167197.
(3) Hanley, S. E.; Cooper, K. F., Sorting nexins in protein homeostasis. *Cells* **2020,** *10* (1), 17.
(4) Petroski, M. D., The ubiquitin system, disease, and drug discovery. *BMC biochemistry* **2008,** *9* (1), 1-15.
(5) Hipp, M. S.; Kasturi, P.; Hartl, F. U., The proteostasis network and its decline in ageing. *Nature reviews Molecular cell biology* **2019,** *20* (7), 421-435.
(6) Chen, X.-Q.; Shen, T.; Fang, S.-J.; Sun, X.-M.; Li, G.-Y.; Li, Y.-F., Protein homeostasis in aging and cancer. *Frontiers in Cell and Developmental Biology* **2023,** *11*, 1143532.
(7) Amm, I.; Sommer, T.; Wolf, D. H., Protein quality control and elimination of protein waste: The role of the ubiquitin–proteasome system. *Biochimica et Biophysica Acta (BBA)-Molecular Cell Research* **2014,** *1843* (1), 182-196.
(8) Ciechanover, A.; Hershko, A.; Rose, I., The Nobel Prize in Chemistry 2004. Nobel Media AB: 2004.
(9) Ciechanover, A.; Orian, A.; Schwartz, A. L., Ubiquitin-mediated proteolysis: biological regulation via destruction. *Bioessays* **2000,** *22* (5), 442-451.
(10) Metzger, M. B.; Hristova, V. A.; Weissman, A. M., HECT and RING finger families of E3 ubiquitin ligases at a glance. *Journal of cell science* **2012,** *125* (3), 531-537.
(11) Pohl, C.; Dikic, I., Cellular quality control by the ubiquitin-proteasome system and autophagy. *Science* **2019,** *366* (6467), 818-822.
(12) Kawahata, I.; Fukunaga, K., Degradation of tyrosine hydroxylase by the ubiquitin-proteasome system in the pathogenesis of Parkinson's disease and dopa-responsive dystonia. *International journal of molecular sciences* **2020,** *21* (11), 3779.
(13) Zheng, N.; Shabek, N., Ubiquitin ligases: structure, function, and regulation. *Annual review of biochemistry* **2017,** *86* (1), 129-157.
(14) Ito, T.; Ando, H.; Suzuki, T.; Ogura, T.; Hotta, K.; Imamura, Y.; Yamaguchi, Y.; Handa, H., Identification of a primary target of thalidomide teratogenicity. *Science* **2010,** *327* (5971), 1345-1350.
(15) Chamberlain, P. P.; Lopez-Girona, A.; Miller, K.; Carmel, G.; Pagarigan, B.; Chie-Leon, B.; Rychak, E.; Corral, L. G.; Ren, Y. J.; Wang, M., Structure of the human Cereblon–DDB1–lenalidomide complex reveals basis for responsiveness to thalidomide analogs. *Nature structural & molecular biology* **2014,** *21* (9), 803-809.
(16) Fischer, E. S.; Böhm, K.; Lydeard, J. R.; Yang, H.; Stadler, M. B.; Cavadini, S.; Nagel, J.; Serluca, F.; Acker, V.; Lingaraju, G. M., Structure of the DDB1–CRBN E3 ubiquitin ligase in complex with thalidomide. *Nature* **2014,** *512* (7512), 49-53.
(17) Collins, G. A.; Goldberg, A. L., The logic of the 26S proteasome. *cell* **2017,** *169* (5), 792-806.
(18) Luh, L. M.; Scheib, U.; Juenemann, K.; Wortmann, L.; Brands, M.; Cromm, P. M., Prey for the proteasome: targeted protein degradation—a medicinal chemist's perspective. *Angewandte Chemie International Edition* **2020,** *59* (36), 15448-15466.
(19) Békés, M.; Langley, D. R.; Crews, C. M., PROTAC targeted protein degraders: the past is prologue. *Nature reviews Drug discovery* **2022,** *21* (3), 181-200.

(20) Schapira, M.; Calabrese, M. F.; Bullock, A. N.; Crews, C. M., Targeted protein degradation: expanding the toolbox. *Nature reviews Drug discovery* **2019,** *18* (12), 949-963.
(21) Xi, J.-Y.; Zhang, R.-Y.; Chen, K.; Yao, L.; Li, M.-Q.; Jiang, R.; Li, X.-Y.; Fan, L., Advances and perspectives of proteolysis targeting chimeras (PROTACs) in drug discovery. *Bioorganic Chemistry* **2022,** *125*, 105848.
(22) Schreiber, S. L., The rise of molecular glues. *cell* **2021,** *184* (1), 3-9.
(23) Gerry, C. J.; Schreiber, S. L., Unifying principles of bifunctional, proximity-inducing small molecules. *Nature chemical biology* **2020,** *16* (4), 369-378.
(24) Stoeckli, E. T., Protocadherins: not just neuron glue, more too! *Developmental cell* **2014,** *30* (6), 643-644.
(25) Ito, T.; Handa, H., Molecular mechanisms of thalidomide and its derivatives. *Proceedings of the Japan Academy, Series B* **2020,** *96* (6), 189-203.
(26) Krönke, J.; Udeshi, N. D.; Narla, A.; Grauman, P.; Hurst, S. N.; McConkey, M.; Svinkina, T.; Heckl, D.; Comer, E.; Li, X., Lenalidomide causes selective degradation of IKZF1 and IKZF3 in multiple myeloma cells. *Science* **2014,** *343* (6168), 301-305.
(27) Lu, G.; Middleton, R. E.; Sun, H.; Naniong, M.; Ott, C. J.; Mitsiades, C. S.; Wong, K.-K.; Bradner, J. E.; Kaelin Jr, W. G., The myeloma drug lenalidomide promotes the cereblon-dependent destruction of Ikaros proteins. *Science* **2014,** *343* (6168), 305-309.
(28) Rehman, W.; Arfons, L. M.; Lazarus, H. M., The rise, fall and subsequent triumph of thalidomide: lessons learned in drug development. *Therapeutic advances in hematology* **2011,** *2* (5), 291-308.
(29) Gandhi, A. K.; Kang, J.; Havens, C. G.; Conklin, T.; Ning, Y.; Wu, L.; Ito, T.; Ando, H.; Waldman, M. F.; Thakurta, A., Immunomodulatory agents lenalidomide and pomalidomide co-stimulate T cells by inducing degradation of T cell repressors I karos and A iolos via modulation of the E 3 ubiquitin ligase complex CRL 4 CRBN. *British journal of haematology* **2014,** *164* (6), 811-821.
(30) Sakamoto, K. M.; Kim, K. B.; Kumagai, A.; Mercurio, F.; Crews, C. M.; Deshaies, R. J., Protacs: Chimeric molecules that target proteins to the Skp1–Cullin–F box complex for ubiquitination and degradation. *Proceedings of the National Academy of Sciences* **2001,** *98* (15), 8554-8559.
(31) Gadd, M. S.; Testa, A.; Lucas, X.; Chan, K.-H.; Chen, W.; Lamont, D. J.; Zengerle, M.; Ciulli, A., Structural basis of PROTAC cooperative recognition for selective protein degradation. *Nature chemical biology* **2017,** *13* (5), 514-521.
(32) Zorba, A.; Nguyen, C.; Xu, Y.; Starr, J.; Borzilleri, K.; Smith, J.; Zhu, H.; Farley, K. A.; Ding, W.; Schiemer, J., Delineating the role of cooperativity in the design of potent PROTACs for BTK. *Proceedings of the National Academy of Sciences* **2018,** *115* (31), E7285-E7292.
(33) Deng, L.; Meng, T.; Chen, L.; Wei, W.; Wang, P., The role of ubiquitination in tumorigenesis and targeted drug discovery. *Signal transduction and targeted therapy* **2020,** *5* (1), 1-28.
(34) Armenti, S. T.; Lohmer, L. L.; Sherwood, D. R.; Nance, J., Repurposing an endogenous degradation system for rapid and targeted depletion of C. elegans proteins. *Development* **2014,** *141* (23), 4640-4647.
(35) Okuhira, K.; Ohoka, N.; Sai, K.; Nishimaki-Mogami, T.; Itoh, Y.; Ishikawa, M.; Hashimoto, Y.; Naito, M., Specific degradation of CRABP-II via cIAP1-mediated ubiquitylation induced by hybrid molecules that crosslink cIAP1 and the target protein. *FEBS letters* **2011,** *585* (8), 1147-1152.
(36) Belcher, B. P.; Ward, C. C.; Nomura, D. K., Ligandability of E3 ligases for targeted protein degradation applications. *Biochemistry* **2021,** *62* (3), 588-600.

(37) Zhou, Q.-Q.; Xiao, H.-T.; Yang, F.; Wang, Y.-D.; Li, P.; Zheng, Z.-G., Advancing targeted protein degradation for metabolic diseases therapy. *Pharmacological Research* **2023,** *188*, 106627.
(38) Lu, J.; Qian, Y.; Altieri, M.; Dong, H.; Wang, J.; Raina, K.; Hines, J.; Winkler, J. D.; Crew, A. P.; Coleman, K., Hijacking the E3 ubiquitin ligase cereblon to efficiently target BRD4. *Chemistry & biology* **2015,** *22* (6), 755-763.
(39) Ottis, P.; Toure, M.; Cromm, P. M.; Ko, E.; Gustafson, J. L.; Crews, C. M., Assessing different E3 ligases for small molecule induced protein ubiquitination and degradation. *ACS chemical biology* **2017,** *12* (10), 2570-2578.
(40) Nabet, B.; Roberts, J. M.; Buckley, D. L.; Paulk, J.; Dastjerdi, S.; Yang, A.; Leggett, A. L.; Erb, M. A.; Lawlor, M. A.; Souza, A., The dTAG system for immediate and target-specific protein degradation. *Nature chemical biology* **2018,** *14* (5), 431-441.
(41) Poirson, J.; Cho, H.; Dhillon, A.; Haider, S.; Imrit, A. Z.; Lam, M. H. Y.; Alerasool, N.; Lacoste, J.; Mizan, L.; Wong, C., Proteome-scale discovery of protein degradation and stabilization effectors. *Nature* **2024,** *628* (8009), 878-886.
(42) Pinch, B. J.; Buckley, D. L.; Gleim, S.; Brittain, S. M.; Tandeske, L.; D'Alessandro, P. L.; Hauseman, Z. J.; Lipps, J.; Xu, L.; Harvey, E. P., A strategy to assess the cellular activity of E3 ligase components against neo-substrates using electrophilic probes. *Cell chemical biology* **2022,** *29* (1), 57-66. e6.
(43) Sakamoto, K.; Hayashi, A.; Sakamoto, A.; Kiga, D.; Nakayama, H.; Soma, A.; Kobayashi, T.; Kitabatake, M.; Takio, K.; Saito, K., Site-specific incorporation of an unnatural amino acid into proteins in mammalian cells. *Nucleic acids research* **2002,** *30* (21), 4692-4699.
(44) Young, D. D.; Schultz, P. G., Playing with the molecules of life. *ACS chemical biology* **2018,** *13* (4), 854-870.
(45) Jann, C.; Giofré, S.; Bhattacharjee, R.; Lemke, E. A., Cracking the code: reprogramming the genetic script in prokaryotes and eukaryotes to harness the power of noncanonical amino acids. *Chemical reviews* **2024,** *124* (18), 10281-10362.
(46) Winter, G. E.; Buckley, D. L.; Paulk, J.; Roberts, J. M.; Souza, A.; Dhe-Paganon, S.; Bradner, J. E., Phthalimide conjugation as a strategy for in vivo target protein degradation. *Science* **2015,** *348* (6241), 1376-1381.
(47) Jang, H. S.; Jana, S.; Blizzard, R. J.; Meeuwsen, J. C.; Mehl, R. A., Access to faster eukaryotic cell labeling with encoded tetrazine amino acids. *Journal of the American Chemical Society* **2020,** *142* (16), 7245-7249.
(48) Nowak, R. P.; DeAngelo, S. L.; Buckley, D.; He, Z.; Donovan, K. A.; An, J.; Safaee, N.; Jedrychowski, M. P.; Ponthier, C. M.; Ishoey, M.; Zhang, T.; Mancias, J. D.; Gray, N. S.; Bradner, J. E.; Fischer, E. S., Plasticity in binding confers selectivity in ligand-induced protein degradation. *Nature chemical biology* **2018,** *14* (7), 706-714.
(49) Mani, R.-S., The emerging role of speckle-type POZ protein (SPOP) in cancer development. *Drug discovery today* **2014,** *19* (9), 1498-1502.
(50) Wei, C.; Liu, Y.; Liu, X.; Cheng, J.; Fu, J.; Xiao, X.; Moses, R. E.; Li, X.; Fu, J., The speckle-type POZ protein (SPOP) inhibits breast cancer malignancy by destabilizing TWIST1. *Cell Death Discovery* **2022,** *8* (1), 389.
(51) Nowak, R. P.; DeAngelo, S. L.; Buckley, D.; He, Z.; Donovan, K. A.; An, J.; Safaee, N.; Jedrychowski, M. P.; Ponthier, C. M.; Ishoey, M., Plasticity in binding confers selectivity in ligand-induced protein degradation. *Nature chemical biology* **2018,** *14* (7), 706-714.
(52) Bednar, R. M.; Jana, S.; Kuppa, S.; Franklin, R.; Beckman, J.; Antony, E.; Cooley, R. B.; Mehl, R. A., Genetic incorporation of two mutually orthogonal bioorthogonal amino

acids that enable efficient protein dual-labeling in cells. *ACS chemical biology* **2021,** *16* (11), 2612-2622.
(53) Eddins, A. J.; Bednar, R. M.; Jana, S.; Pung, A. H.; Mbengi, L.; Meyer, K.; Perona, J. J.; Cooley, R. B.; Karplus, P. A.; Mehl, R. A., Truncation-free genetic code expansion with tetrazine amino acids for quantitative protein ligations. *Bioconjugate Chemistry* **2023,** *34* (12), 2243-2254.
(54) Xu, L.; Chen, Y.; Mayakonda, A.; Koh, L.; Chong, Y. K.; Buckley, D. L.; Sandanaraj, E.; Lim, S. W.; Lin, R. Y.-T.; Ke, X.-Y., Targetable BET proteins-and E2F1-dependent transcriptional program maintains the malignancy of glioblastoma. *Proceedings of the National Academy of Sciences* **2018,** *115* (22), E5086-E5095.
(55) Smalley, J. P.; Baker, I. M.; Pytel, W. A.; Lin, L.-Y.; Bowman, K. J.; Schwabe, J. W.; Cowley, S. M.; Hodgkinson, J. T., Optimization of class I histone deacetylase PROTACs reveals that HDAC1/2 degradation is critical to induce apoptosis and cell arrest in cancer cells. *Journal of medicinal chemistry* **2022,** *65* (7), 5642-5659.
(56) Moreau, K.; Coen, M.; Zhang, A. X.; Pachl, F.; Castaldi, M. P.; Dahl, G.; Boyd, H.; Scott, C.; Newham, P., Proteolysis-targeting chimeras in drug development: a safety perspective. *British journal of pharmacology* **2020,** *177* (8), 1709-1718.
(57) Dai, X.; Gan, W.; Li, X.; Wang, S.; Zhang, W.; Huang, L.; Liu, S.; Zhong, Q.; Guo, J.; Zhang, J., Prostate cancer–associated SPOP mutations confer resistance to BET inhibitors through stabilization of BRD4. *Nature medicine* **2017,** *23* (9), 1063-1071.
(58) Zhang, P.; Wang, D.; Zhao, Y.; Ren, S.; Gao, K.; Ye, Z.; Wang, S.; Pan, C.-W.; Zhu, Y.; Yan, Y., Intrinsic BET inhibitor resistance in SPOP-mutated prostate cancer is mediated by BET protein stabilization and AKT–mTORC1 activation. *Nature medicine* **2017,** *23* (9), 1055-1062.
(59) Janouskova, H.; El Tekle, G.; Bellini, E.; Udeshi, N. D.; Rinaldi, A.; Ulbricht, A.; Bernasocchi, T.; Civenni, G.; Losa, M.; Svinkina, T., Opposing effects of cancer-type-specific SPOP mutants on BET protein degradation and sensitivity to BET inhibitors. *Nature medicine* **2017,** *23* (9), 1046-1054.
(60) Ostertag, M. S.; Hutwelker, W.; Plettenburg, O.; Sattler, M.; Popowicz, G. M., Structural insights into BET client recognition of endometrial and prostate cancer-associated SPOP mutants. *Journal of molecular biology* **2019,** *431* (11), 2213-2221.
(61) Zhuang, M.; Calabrese, M. F.; Liu, J.; Waddell, M. B.; Nourse, A.; Hammel, M.; Miller, D. J.; Walden, H.; Duda, D. M.; Seyedin, S. N., Structures of SPOP-substrate complexes: insights into molecular architectures of BTB-Cul3 ubiquitin ligases. *Molecular cell* **2009,** *36* (1), 39-50.
(62) Halgren, T. A., Identifying and characterizing binding sites and assessing druggability. *Journal of chemical information and modeling* **2009,** *49* (2), 377-389.
(63) Wang, D.; Ma, J.; Botuyan, M. V.; Cui, G.; Yan, Y.; Ding, D.; Zhou, Y.; Krueger, E. W.; Pei, J.; Wu, X., ATM-phosphorylated SPOP contributes to 53BP1 exclusion from chromatin during DNA replication. *Science Advances* **2021,** *7* (25), eabd9208.
(64) Nikhil, K.; Haymour, H. S.; Kamra, M.; Shah, K., Phosphorylation-dependent regulation of SPOP by LIMK2 promotes castration-resistant prostate cancer. *British Journal of Cancer* **2021,** *124* (5), 995-1008.
(65) Oprea, T. I.; Bologa, C. G.; Brunak, S.; Campbell, A.; Gan, G. N.; Gaulton, A.; Gomez, S. M.; Guha, R.; Hersey, A.; Holmes, J., Unexplored therapeutic opportunities in the human genome. *Nature reviews Drug discovery* **2018,** *17* (5), 317-332.
(66) Bridge, T.; Wegmann, U.; Crack, J. C.; Orman, K.; Shaikh, S. A.; Farndon, W.; Martins, C.; Saalbach, G.; Sachdeva, A., Site-specific encoding of photoactivity and photoreactivity into antibody fragments. *Nature chemical biology* **2023,** *19* (6), 740-749.

(67) Huguenin-Dezot, N.; Alonzo, D. A.; Heberlig, G. W.; Mahesh, M.; Nguyen, D. P.; Dornan, M. H.; Boddy, C. N.; Schmeing, T. M.; Chin, J. W., Trapping biosynthetic acyl-enzyme intermediates with encoded 2, 3-diaminopropionic acid. *Nature* **2019,** *565* (7737), 112-117.
(68) Devaraj, N.; Upadhyay, R.; Haun, J.; Hilderbrand, S.; Weissleder, R., Fast and Sensitive Pretargeted Labeling of Cancer Cells through a Tetrazine/trans. *Angew. Chem., Int. Ed.* **2010,** *49*, 2869 —2872.
(69) de Almeida, G.; Sletten, E. M.; Nakamura, H.; Palaniappan, K. K.; Bertozzi, C. R., Thiacycloalkynes for copper-free click chemistry. *Angewandte Chemie (International ed. in English)* **2012,** *51* (10), 2443.
(70) Best, M. D., Click chemistry and bioorthogonal reactions: unprecedented selectivity in the labeling of biological molecules. *Biochemistry* **2009,** *48* (28), 6571-6584.
(71) Blizzard, R. J.; Backus, D. R.; Brown, W.; Bazewicz, C. G.; Li, Y.; Mehl, R. A., Ideal bioorthogonal reactions using a site-specifically encoded tetrazine amino acid. *Journal of the American Chemical Society* **2015,** *137* (32), 10044-10047.
(72) Darko, A.; Wallace, S.; Dmitrenko, O.; Machovina, M. M.; Mehl, R. A.; Chin, J. W.; Fox, J. M., Conformationally strained trans-cyclooctene with improved stability and excellent reactivity in tetrazine ligation. *Chemical science* **2014,** *5* (10), 3770-3776.
(73) Crowe, C.; Nakasone, M. A.; Chandler, S.; Craigon, C.; Sathe, G.; Tatham, M. H.; Makukhin, N.; Hay, R. T.; Ciulli, A., Mechanism of degrader-targeted protein ubiquitinability. *Science Advances* **2024,** *10* (41), eado6492.
(74) Shade, O.; Ryan, A.; Belsito, G.; Deiters, A., Investigating protein degradability through site-specific ubiquitin ligase recruitment. *RSC Chemical Biology* **2025,** *6* (2), 240-248.
(75) Xiao, Z.; Gavriil, E. S.; Cao, F.; Zhang, X.; Li, S. X.; Kotelnikov, S.; Michalska, P.; Marte, F.; Huang, C.; Lu, Y., Identification of actionable targeted protein degradation effector sites through Site-specific Ligand Incorporation-induced Proximity (SLIP). *bioRxiv* **2025**, 2025.02. 04.636303.
(76) Osgood, A. O.; Huang, Z.; Szalay, K. H.; Chatterjee, A., Strategies to Expand the Genetic Code of Mammalian Cells. *Chemical reviews* **2025**.
(77) Dunkelmann, D. L.; Chin, J. W., Engineering pyrrolysine systems for genetic code expansion and reprogramming. *Chemical reviews* **2024,** *124* (19), 11008-11062.
(78) Tran, N. L.; Leconte, G. A.; Ferguson, F. M., Targeted protein degradation: design considerations for PROTAC development. *Current protocols* **2022,** *2* (12), e611.
(79) Winter, G. E.; Mayer, A.; Buckley, D. L.; Erb, M. A.; Roderick, J. E.; Vittori, S.; Reyes, J. M.; di Iulio, J.; Souza, A.; Ott, C. J., BET bromodomain proteins function as master transcription elongation factors independent of CDK9 recruitment. *Molecular cell* **2017,** *67* (1), 5-18. e19.
(80) Abramson, J.; Adler, J.; Dunger, J.; Evans, R.; Green, T.; Pritzel, A.; Ronneberger, O.; Willmore, L.; Ballard, A. J.; Bambrick, J., Accurate structure prediction of biomolecular interactions with AlphaFold 3. *Nature* **2024**, 1-3.
(81) Angers, S.; Li, T.; Yi, X.; MacCoss, M. J.; Moon, R. T.; Zheng, N., Molecular architecture and assembly of the DDB1–CUL4A ubiquitin ligase machinery. *Nature* **2006,** *443* (7111), 590-593.
(82) Matyskiela, M. E.; Lu, G.; Ito, T.; Pagarigan, B.; Lu, C.-C.; Miller, K.; Fang, W.; Wang, N.-Y.; Nguyen, D.; Houston, J., A novel cereblon modulator recruits GSPT1 to the CRL4CRBN ubiquitin ligase. *Nature* **2016,** *535* (7611), 252-257.
(83) Moriarty, N. W.; Grosse-Kunstleve, R. W.; Adams, P. D., electronic Ligand Builder and Optimization Workbench (eLBOW): a tool for ligand coordinate and restraint generation. *Acta Crystallographica Section D: Biological Crystallography* **2009,** *65* (10), 1074-1080.

(84) Filippakopoulos, P.; Qi, J.; Picaud, S.; Shen, Y.; Smith, W. B.; Fedorov, O.; Morse, E. M.; Keates, T.; Hickman, T. T.; Felletar, I., Selective inhibition of BET bromodomains. *Nature* **2010,** *468* (7327), 1067-1073.